ACS APPLIED MATERIALS & INTERFACES

Research Article

www.acsami.org

Microwave-Assisted Self-Doping of TiO_2 Photonic Crystals for Efficient Photoelectrochemical Water Splitting

Zhonghai Zhang,[†] Xiulin Yang,[†] Mohamed Nejib Hedhili,[‡] Elaf Ahmed,[†] Le Shi,[†] and Peng Wang*[,†]

[†]Water Desalination and Reuse Center, Biological and Environmental Science and Engineering Division and [‡]Imaging and Characterization Laboratory, King Abdullah University of Science and Technology, Thuwal 23955-6900, Saudi Arabia

Supporting Information

ABSTRACT: In this article, we report that the combination of microwave heating and ethylene glycol, a mild reducing agent, can induce Ti^{3+} self-doping in TiO_2. A hierarchical TiO_2 nanotube array with the top layer serving as TiO_2 photonic crystals (TiO_2 NTPCs) was selected as the base photoelectrode. The self-doped TiO_2 NTPCs demonstrated a 10-fold increase in visible-light photocurrent density compared to the nondoped one, and the optimized saturation photocurrent density under simulated AM 1.5G illumination was identified to be 2.5 mA cm^{-2} at 1.23 V versus reversible hydrogen electrode, which is comparable to the highest values ever reported for TiO_2-based photoelectrodes. The significant enhancement of photoelectrochemical performance can be ascribed to the rational coupling of morphological and electronic features of the self-doped TiO_2 NTPCs: (1) the periodically morphological structure of the photonic crystal layer traps broadband visible light, (2) the electronic interband state induced from self-doping of Ti^{3+} can be excited in the visible-light region, and (3) the captured light by the photonic crystal layer is absorbed by the self-doped interbands.

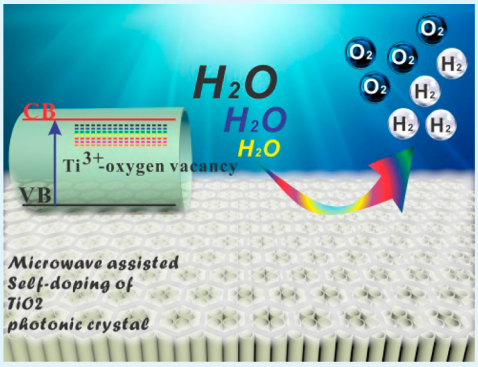

KEYWORDS: *self-doping, TiO_2 nanotube, photonic crystal, photoelectrochemical, water splitting*

1. INTRODUCTION

In situ self-doping with homospecies, Ti^{3+}, is regarded as one of the promising strategies to enhance the photoelectrochemical (PEC) performance of TiO_2-based photoelectrodes.[1−4] The self-doping method does not involve significant structural disturbance and thus leads to reduced defect formation as compared with heteroelements doping (e.g., C, N, and F).[5−9] The Ti^{3+} self-doped TiO_2 photoelectrodes have demonstrated both improved visible-light absorption because of the interband states of the Ti^{3+} oxygen vacancy and increased electrical conductivity because of the high donor density, leading to enhanced PEC performance within both the visible and UV-light regions.[10,11]

The previously reported TiO_2 self-doping methods were focused mainly on hydrogenation,[12−15] heating in reducing gas (CO or NO),[16] laser irradiation,[17] and high-energy-particle bombardment (Ar^+ ions or electrons),[18,19] all of which necessitated harsh synthetic conditions or expensive facilities. Ye et al. reported a chemical reduction method to synthesize reduced TiO_2 in which sodium borohydride, a toxic and harsh reducing agent, was involved.[20] Hence, developing a simple, environmentally friendly, and economical strategy to synthesize a stable Ti^{3+} self-doped TiO_2-based photoelectrode is still a big challenge. Very recently, our group developed a versatile electrochemical-induced Ti^{3+} self-doping strategy, and a significant enhancement in PEC performance was achieved under stimulated solar light, whereas the performance under visible light needed further improvement.[21]

In the present work, we report that the combination of microwave heating and ethylene glycol (EG), a mild reducing agent, can induce Ti^{3+} self-doping in TiO_2. Microwave heating has recently attracted significant interest in the field of material synthesis owing to its fast and well-controlled heating rate, homogenous heat distribution, and energy efficiency.[22−25] Typically, the heating task that requires several hours to complete under conventional heating (e.g., oven heating and oil-bath heating) can be achieved within minutes under microwave heating. EG was selected because of its good reduction activity under heating, nonflammability, and environmentally friendly properties.[26] A hierarchical TiO_2 nanotube array with the top layer serving as TiO_2 photonic crystals (TiO_2 NTPCs), which are able to trap visible light, was selected as the base photoelectrode to enhance further its visible-light PEC performance. The TiO_2 NTPCs were synthesized by a facile two-step anodization method and then self-doped through EG reduction in a microwave process (MWR-TiO_2 NTPCs).

2. EXPERIMENTAL SECTION

2.1. Chemicals and Materials. A 2 mm thick titanium sheet (99.6%, Strem Chemicals) was cut into pieces of 25 × 10 mm^2. Ethylene glycol (EG), ammonia fluoride (NH_4F), and potassium hydroxide (KOH) were purchased from Acros Organics and used as

Received: October 31, 2013
Accepted: December 16, 2013
Published: December 16, 2013

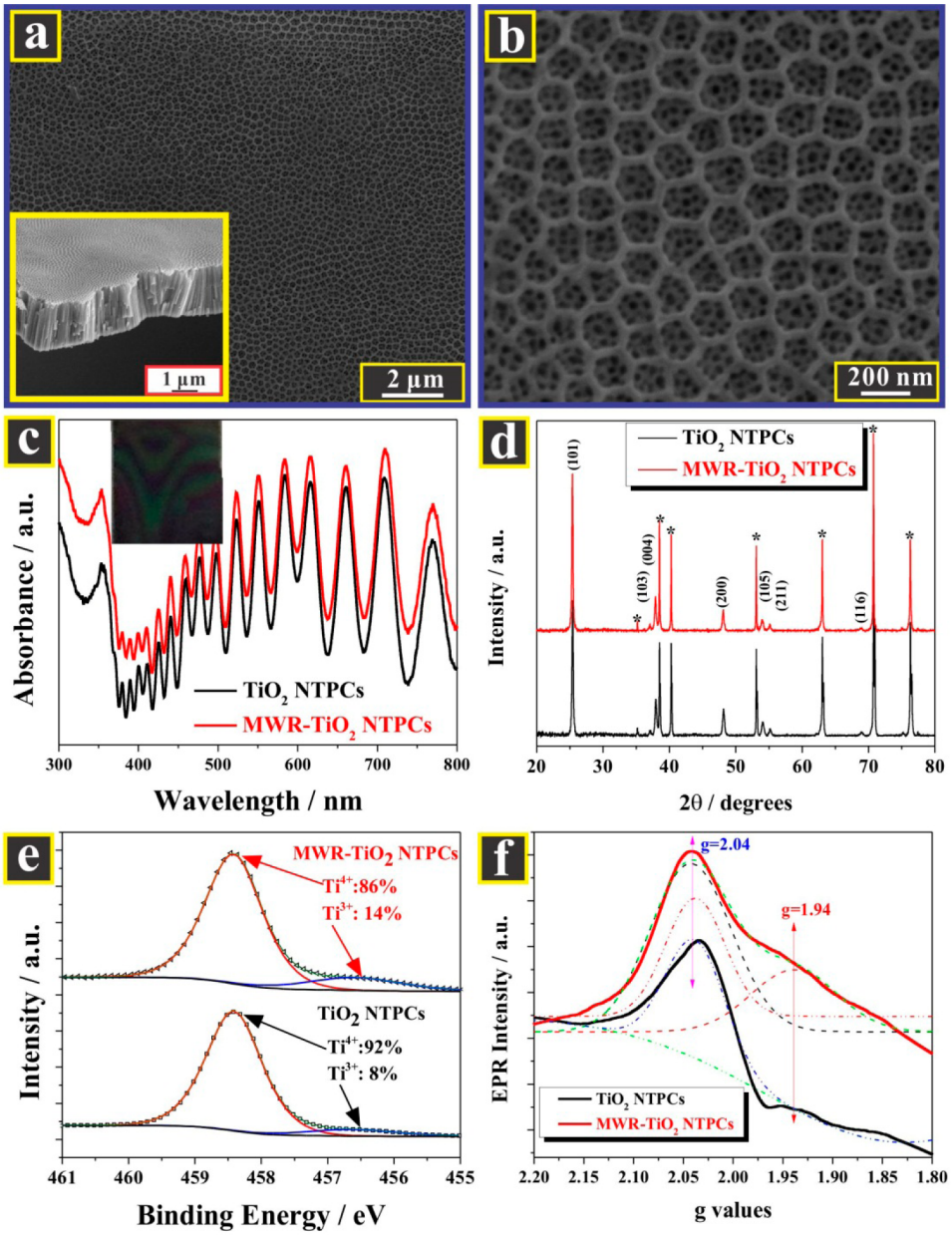

Figure 1. SEM images of the (a) large-scale top view of the MWR-TiO_2 NTPCs; the inset shows a cross-sectional view with top-ring/bottom-tube structures and (b) high-magnification top view of the MWR-TiO_2 NTPCs. (c) UV−vis diffuse reflectance absorption spectra of the TiO_2 NTPCs and MWR-TiO_2 NTPCs; the inset presents a digital photo of the MWR-TiO_2 NTPCs. (d) XRD patterns of the TiO_2 NTPCs and MWR-TiO_2 NTPCs. (e) XPS core level of Ti $2p_{3/2}$ after argon sputtering of the TiO_2 NTPCs and MWR-TiO_2 NTPCs. (f) EPR spectra of the TiO_2 NTPCs and MWR-TiO_2 NTPCs.

received. All aqueous solutions were prepared using deionized (DI) water with a resistivity of 18.2 MΩ cm prepared by a Millipore system.

2.2. Preparation of the MWR-TiO_2 NTPCs. The hierarchical TiO_2 NTPCs were fabricated by a two-step anodization process. Prior to anodization, the Ti sheets were first degreased by sonicating in ethanol and room-temperature DI water followed by drying in a pure nitrogen stream. The anodization was carried out using a conventional two-electrode system with the Ti sheet as the anode and Pt mesh (Aldrich, 100 mesh) as the cathode, respectively. All electrolytes consisted of 0.65 wt % NH_4F (the concentration of NH_4F used in this study was higher than in our previously work (0.50 wt %)[21] because it was found that a higher concentration of NH_4F was helpful for increasing the uniformity of the TiO_2 NTPCs) in EG solution with 2% (v/v) water. All anodization was carried out at room temperature. In the first step of the anodization, the Ti sheet was anodized at 60 V for 30 min, and then the as-grown nanotube layer was ultrasonically removed in DI water. The same Ti sheet then underwent the second anodization at 20 V for 30 min, then 25 V for 30 min, and finally, 30 V for 30 min. After the two-step anodization, the prepared TiO_2 NTPCs samples were cleaned with DI water and dried with N_2 gas. The as-anodized TiO_2 NTPCs was annealed in air at 450 °C for 1 h with a heating rate of 5 °C min^{-1}. The TiO_2 NTPCs was put into a microwave vials with 6 mL EG and heated with a of Biotage Initiator microwave synthesizer for 2−180 min (Figure S1).

2.3. Characterization of the MWR-TiO_2 NTPCs. The morphologies of the TiO_2 NTPCs and MWR-TiO_2 NTPCs were determined by field-emission scanning electron microscopy (FESEM, FEI Quanta 600). The crystalline structure of the samples was analyzed by X-ray diffraction (XRD, Bruker D8 Discover diffractometer, using Cu Kα radiation, λ = 1.540598 Å). The diffuse reflectance UV−vis adsorption spectra were recorded on a spectrophotometer (Shimadazu, UV 2550), with fine $BaSO_4$ powder

dx.doi.org/10.1021/am404848n | ACS Appl. Mater. Interfaces 2014, 6, 691−696

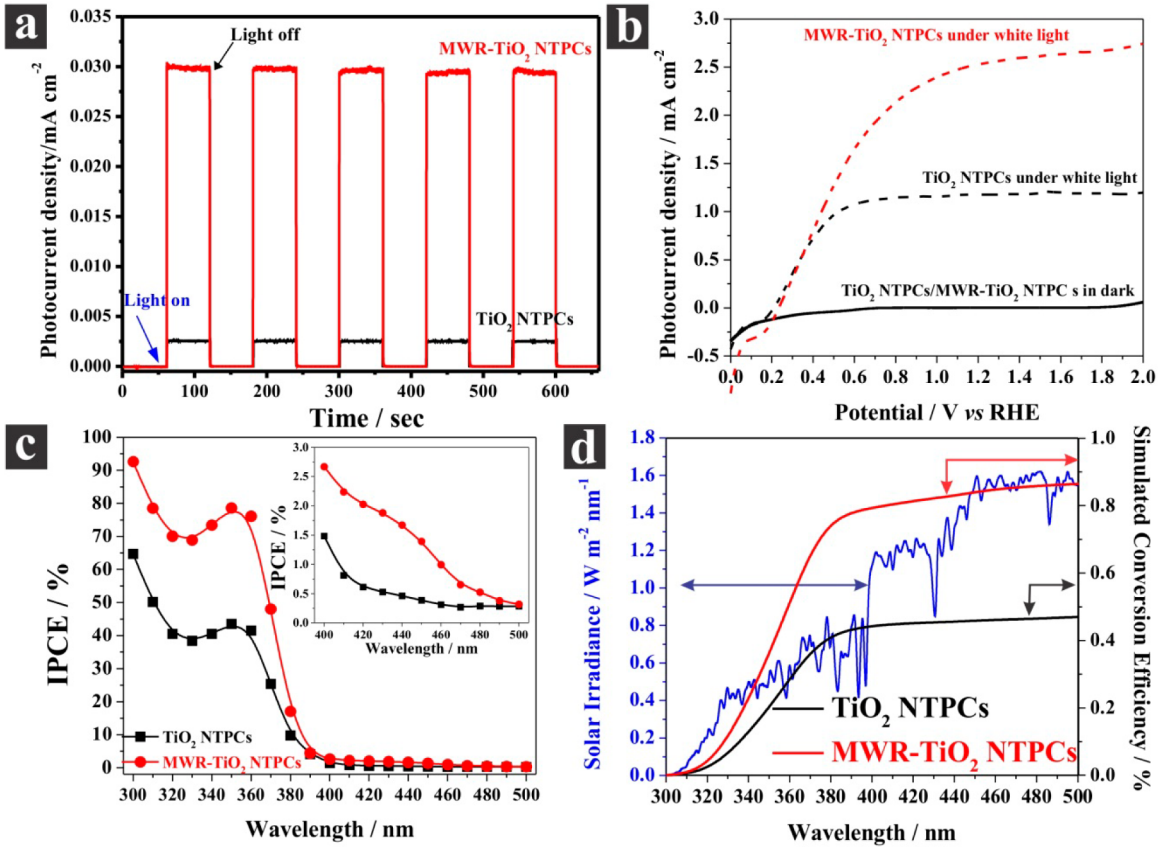

Figure 2. PEC performance of the TiO_2 NTPCs and MWR-TiO_2 NTPCs photoelectrodes: (a) amperometric transient photocurrent density vs time plots at an applied potential of 1.23 V vs RHE under illumination of visible light with wavelengths ≥420 nm and 60 s light on/off cycles. (b) Linear-sweep voltammograms collected with a scan rate of 5 mV s^{-1} under simulated solar light (AM 1.5G). (c) IPCE plots collected at an incident wavelength range from 300 to 500 nm without external bias; the inset is the magnified IPCE spectra at an incident wavelength range from 400 to 500 nm. (d) Photoconversion efficiency for the TiO_2 NTPCs and MWR-TiO_2 NTPCs as a function of wavelength by integrating their IPCE spectra with a standard AM 1.5G solar spectrum (ASTM G-173-03).

as reference. The electron paramagnetic resonance (EPR) spectra were recorded on a Bruker E500-10/12: ELEXSYS EPR spectrometer. Photoelectron spectroscopy (XPS) data were collected by an Axis Ultra instrument (Kratos Analytical) under ultrahigh vacuum ($<10^{-8}$ Torr) and using a monochromatic Al Kα X-ray source operating at 150 W. The survey and high-resolution spectra were collected at fixed analyzer pass energies of 160 and 20 eV, respectively. Binding energies were referenced to the C 1s binding energy of adventitious-carbon contamination, which was set at 284.8 eV. Argon sputtering at 500 eV for 30 s was employed to remove the oxidized top surface layer of the TiO_2 NTPCs and MWR-TiO_2 NTPCs before analyzing Ti^{3+} in the bulk phase.

2.4. PEC Performance of the MWR-TiO_2 NTPCs. The PEC performance of the TiO_2 NTPCs and MWR-TiO_2 NTPCs was evaluated using a three-electrode configuration with the TiO_2 NTPCs or MWR-TiO_2 NTPCs, Ag/AgCl, and Pt mesh as the working, reference, and counter electrodes, respectively. The supporting electrolyte was a 1 M KOH solution. The potentials of the photoelectrodes were controlled by a potentiostat and were reported against a reversible hydrogen electrode (RHE) using the following equation[27]

$$E_{RHE} = E_{Ag/AgCl} + 0.059\ pH + E^{\circ}_{Ag/AgCl} \quad (1)$$

where $E^{\circ}_{Ag/AgCl}$ = 0.1976 V at 25 °C. The scan rate for the linear-sweep voltammetry (LSV) was 5 mV s^{-1}. The transient photoresponse was evaluated under chopped-light irradiation (light on/off cycles: 60 s) at a fixed electrode potential of 1.23 V versus RHE. The photocurrent was measured under irradiation from a 300 W Xe lamp (PLS-SXE300, PE300BF). The intensity of the light source was calibrated with a Si diode (Model 818, Newport) to simulate AM 1.5G illumination (100 mW cm^{-2}). The incident-photon-to-current-conversion efficiency (IPCE) measurements were performed without external bias in a two-electrode model, with TiO_2 NTPCs/MWR-TiO_2 NTPCs as the anode and Pt mesh as the cathode. The electrochemical impedance spectra (EIS) were measured using a PGSTAT 302N Autolab Potentiostat/Galvanostat (Metrohm) equipped with a frequency-analyzer module (FRA2) with an excitation signal of 10 mV amplitude. The impedance versus frequency spectra were acquired at the open circular potential of the system both in the dark and under illumination conditions. Afterward, an impedance versus potential measurement at a fixed frequency of 5k Hz in the dark was performed to determine the carrier density.

3. RESULTS AND DISCUSSION

The large-scale and high-magnification top-view scanning electron microscope (SEM) images of the MWR-TiO_2 NTPCs are presented in Figure 1, panels a and b, respectively, and a periodical nano-ring structure with a diameter in the range of 150−200 nm was observed, which does not show significant morphological differences after the MWR process compared to the TiO_2 NTPCs (the SEM image of the TiO_2 NTPCs is presented in Figure S2). The inset in Figure 1a presents a high-magnification cross-sectional SEM image of the MWR-TiO_2 NTPCs, which confirms the hierarchical top-ring/bottom-tube nanostructures, with the top-layer thickness being ~70 nm and a tube length of around ~2.0 μm. The unique top photonic crystal (PC) layer and bottom 1D nanotube structure

dx.doi.org/10.1021/am404848n | ACS Appl. Mater. Interfaces 2014, 6, 691−696

is beneficial for (1) broadband light confinement and (2) unidirectional electron transport. The UV−vis diffuse reflectance absorption spectra of the TiO_2 NTPCs and MWR-TiO_2 NTPCs were measured and are presented in Figure 1c, from which multiabsorption peaks can be clearly observed in visible-light region. For the self-doping Ti^{3+} with MWR, the multiabsorption peak positions did not change significantly, and the optical-absorption intensity was further enhanced. The inset in Figure 1c shows an actual photo of MWR-TiO_2 NTPCs, and a visual color pattern was observed, which provides macroscopic evidence of the formation of a PC layer. The X-ray diffraction (XRD) profiles of the TiO_2 NTPCs and MWR-TiO_2 NTPCs are presented in Figure 1d. Clearly, the strong XRD diffraction peaks at 25.3° indicate a vastly dominant anatase phase with a preferential orientation of (101) both for the TiO_2 NTPCs and MWR-TiO_2 NTPCs (JCPDS no. 21-1272), and no difference in the XRD peaks was observed after the MWR process.

To examine the surface chemical bonding of the TiO_2 NTPCs and MWR-TiO_2 NTPCs, X-ray photoelectron spectroscopy (XPS) was employed, and the XPS survey spectra are shown in Figure S3a. The core level Ti $2p_{3/2}$ XPS of the TiO_2 NTPCs and MWR-TiO_2 NTPCs were not significantly different (Figure S3b), as the Ti^{3+} species on the surface can be easily oxidized back to Ti^{4+} by oxygen in air. In this work, we employed an argon-sputtering treatment, as reported in our previous work,[21] to remove the top surface layer of the TiO_2 under high-vacuum conditions before XPS measurement to probe the Ti^{3+} in material's bulk phase. The high-resolution core-level Ti $2p_{3/2}$ spectra of the TiO_2 NTPCs and MWR-TiO_2 NTPCs after argon-sputtering treatment are presented in Figure 1e. After fitting, the dominant peak centered at 458.5 eV is associated with Ti ions with a formal valence of four (Ti^{4+}), whereas the peak at the lower binding energy of 456.6 eV is associated with Ti ions with reduced charge state (Ti^{3+}).[28] The abundance of Ti^{3+} detected in the MWR-TiO_2 NTPCs was ∼14%, whereas that in the TiO_2 NTPCs was ∼8%. The increased Ti^{3+} abundance in the MWR-TiO_2 NTPCs corresponds to the bulk Ti^{3+} created in the MWR process. To confirm the successful self-doping of Ti^{3+} further, electron paramagnetic resonance (EPR) spectra were recorded and are provided in Figure 1f. The TiO_2 NTPCs show a strong single EPR signal with g = 2.04, which can be ascribed to the absorbents on the TiO_2 surface, such as O^- or O_2^- radicals.[29] Besides the signal at g = 2.04, the MWR-TiO_2 NTPCs sample shows an EPR signal with g = 1.94, which can be ascribed to the existence of Ti^{3+}.[30−32] After the MWR process, an oxygen atom at the bridging O site escaped and left behind oxygen vacancies, which created excess electrons, giving rise to Ti^{3+} ions.

Transient photocurrent response measurements were carried out on the TiO_2 NTPCs and MWR-TiO_2 NTPCs during repeated on/off visible-light-illumination cycles at 1.23 V versus RHE (Figure 2a). The results show that both samples exhibited fast and reproducible photocurrent responses upon each illumination. The transient photocurrent density of the TiO_2 NTPCs was 0.0030 mA cm^{-2}, whereas that of the MWR-TiO_2 NTPCs was 0.030 mA cm^{-2}, which represents a 10-fold increase from the pristine TiO_2 NTPCs. The PEC performance of the TiO_2 NTs and MWR-TiO_2 NTs without the photonic crystal layer was also measured, and photocurrent densities of 0.0025 and 0.008 mA cm^{-2}, respectively, were recorded under the same experimental conditions (Figure S4a).

To measure the PEC performances under simulated solar-light illumination of AM 1.5G (100 mW cm^{-2}) further, linear-sweep voltammetry (LSV) of the TiO_2 NTPCs and MWR-TiO_2 NTPCs was recorded, and the data are presented in Figure 2b. No significant dark current was observed even at high potentials (2.0 V vs RHE) on both the TiO_2 NTPCs and MWR-TiO_2 NTPCs photoelectrodes, whereas high photocurrent densities were recorded for them under illumination. Clearly, the MWR-TiO_2 NTPCs showed a much higher photocurrent density (2.5 mA cm^{-2} at 1.23 V vs RHE) than that of the pristine TiO_2 NTPCs (1.2 mA cm^{-2} at 1.23 V vs RHE), which represents a 108% increase in PEC performance. In addition, the PEC performance of the TiO_2 NTs and MWR-TiO_2 NTs under illumination of simulated solar light was also measured, and much lower photocurrent densities of 0.39 and 0.57 mA cm^{-2}, respectively, were recorded (Figure S4b).

The effects of the microwave-heating duration on the final PEC performance of the prepared MWR-TiO_2 NTPCs were also investigated, and the results are presented in Figure S5. Clearly, with only 5 min of MWR treatment, the MWR-TiO_2 NTPCs reached their optimized PEC performance, and any further extension of the heating time did not result in a further increase in the photocurrent density and photoconversion efficiency. This result demonstrates the fascinating fast heating property of microwave heating.

Incident-photon-to-current-conversion efficiency (IPCE) measurements were performed on the TiO_2 NTPCs and MWR-TiO_2 NTPCs separately, and the IPCE values were calculated using the following equation and are presented in Figure 2c[33]

$$\mathrm{IPCE}\% = \left(\frac{1240I}{\lambda J_{\mathrm{light}}}\right)100 \tag{2}$$

where I is the photocurrent density, J_{light} is the incident-light irradiance, and λ is the incident-light wavelength. In comparison to the TiO_2 NTPCs, the MWR-TiO_2 NTPCs exhibited considerably enhanced photo-activity over both the UV and visible-light regions, which agreed well with the PEC results. The magnified IPCE spectra from 400 to 500 nm are presented in the inset of Figure 2c, and the MWR-TiO_2 NTPCs demonstrated enhanced IPCE performance within the visible-light region. Furthermore, the IPCE discrepancy versus wavelength between the TiO_2 NTPCs and MWR-TiO_2 NTPCs were also calculated, and the correlation between UV−vis absorption and IPCE data are presented in Figure S6. The enhancement in the IPCE was largely consistent with the increased light-absorption spectrum and thus the photoresponse of the doped samples not only resulted from the intrinsic excitation of the valence band electrons to the conduction band but also involved the interbands induced by the self-doped Ti^{3+}.[34]

To calculate the photoconversion efficiency and to eliminate the discrepancy between the irradiance of the light source used in lab and the actual solar-light spectrum, the corresponding IPCE spectra were integrated with a standard AM 1.5G solar spectrum (ASTM G-173-03) using the following equation[33]

$$\eta\% = \int_{300}^{500} \frac{1}{1240}\lambda E^0 \mathrm{IPCE}(\lambda)\, P(\lambda)\, \mathrm{d}(\lambda) \tag{3}$$

where λ is the wavelength of solar light, $P(\lambda)$ is the solar irradiance at a special wavelength, and E^0 is the redox potential

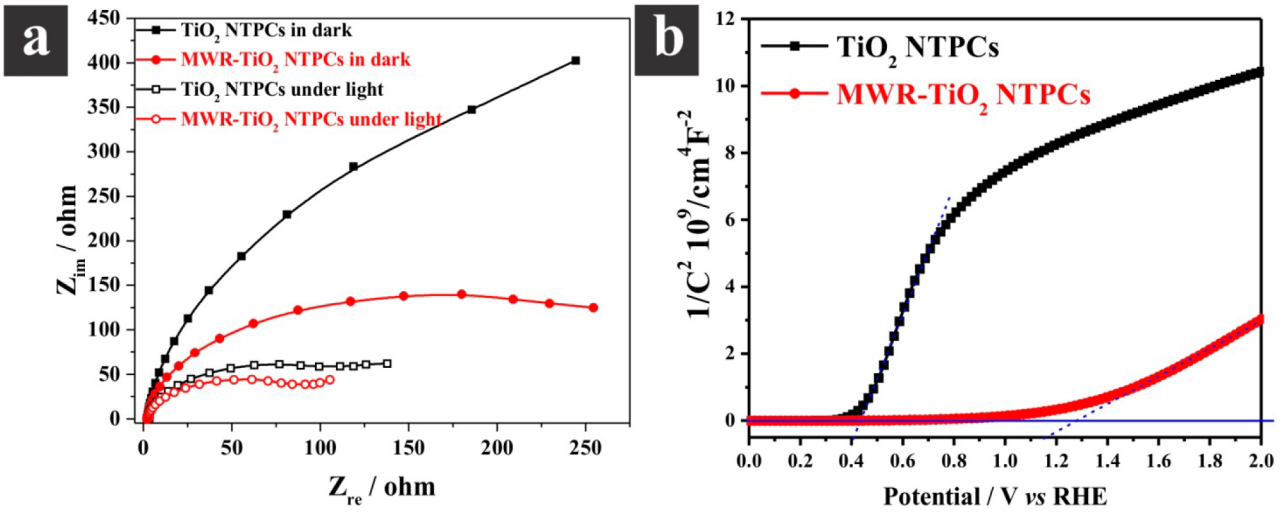

Figure 3. (a) Electrochemical impedance spectra of Nyquist plots (Z_{re} vs Z_{im}) in the dark and under light and (b) Mott−Schottky plots at a fixed frequency of 5 kHz in the dark of TiO_2 NTPCs and MWR-TiO_2 NTPCs.

of water. Figure 2d presents the thus-calculated photoconversion efficiencies as a function of wavelength in the range of 300 to 500 nm, and it can be seen that the TiO_2 NTPCs and MWR-TiO_2 NTPCs achieved photoconversion efficiencies of 0.47 and 0.87%, respectively. The stability of photoelectrodes is an important factor for their practical application, and our MWR-TiO_2 NTPCs sample showed a very stable PEC performance after 120 min of testing (Figure S7), which presumably can be ascribed to the fact that the self-doped Ti^{3+} was largely retained in the bulk phase of the MWR-TiO_2 NTPCs.

To characterize the electronic properties of the TiO_2 NTPCs and MWR-TiO_2 NTPCs further, electrochemical impedance spectra (EIS) measurements were carried out covering the frequency of 10^5 to 0.1 Hz using an amplitude of 10 mV at the open-circuit potential of the system in the dark and under illumination, and the Nyquist plots are presented in Figure 3a. Semicircles in Nyquist plots convey information on the charge-transfer process because the diameters of the semicircles are equal to the charge-transfer resistance of a sample.[35] As depicted in Figure 3a, the MWR-TiO_2 NTPCs exhibited a smaller semicircular diameter than the TiO_2 NTPCs both in the dark and under illumination, implying enhanced electronic conductivity in the MWR-TiO_2 NTPC. Mott−Schottky (MS) plots were collected at 5 kHz to determine the semiconductor type, flat-band potential (U_{FB}), and carrier density (N_D) of the TiO_2 NTPCs and MWR-TiO_2 NTPCs using the following equation[36]

$$\frac{1}{C^2} = \frac{2}{N_D e \varepsilon_0 \varepsilon}\left[(U_S - U_{FB}) - \frac{k_B T}{e}\right] \quad (4)$$

where C is the space charge capacitance in the semiconductor; N_D is the electron carrier density, e is the elementary charge value, ε^0 is the permittivity of the vacuum, ε is the relative permittivity of the semiconductor, U_s is the applied potential, T is temperature, and k_B is the Boltzmann constant. Figure 3b presents the Mott−Schottky (MS) plot as $1/C^2$ versus potential. The slopes of the linear part of the curves in the MS plots were positive, implying that the self-doping of Ti^{3+} did not change the n-type semiconductor property of TiO_2. The linear parts of the curves were extrapolated to $1/C^2 = 0$, and from eq 4, the values of U_{FB} were estimated to be 0.40 and 1.18 V versus RHE for the TiO_2 NTPCs and MWR-TiO_2 NTPCs, respectively. The carrier density, N_D, was determined from Figure 3b using the following equation[36,37]

$$N_D = -\left(\frac{2}{e\varepsilon\varepsilon_0}\right)\left(\frac{d\left(\frac{1}{C^2}\right)}{d(U_s)}\right)^{-1} \quad (5)$$

with $e = -1.6 \times 10^{-19}$, $\varepsilon^0 = 8.86 \times 10^{-12}$, and $\varepsilon = 48$ for anatase TiO_2.[38] The pristine TiO_2 NTPCs showed a N_D of 1.55×10^{18} cm^{-3}, whereas the MWR-TiO_2 NTPCs showed a much higher N_D of 7.03×10^{18} cm^{-3}. The significantly increased carrier density after MWR self-doping of Ti^{3+} would result in a positive shift of the Fermi level, increase in the degree of band bending at the TiO_2 surface (causing the positive shift of the flat-band potential), and finally, facilitate the charge separation at the semiconductor/electrolyte interface.[21]

The electron lifetime in the TiO_2 NTPCs and MWR-TiO_2 NTPCs was also measured through open-circuit photovoltage decay,[39] presented in Figure S8, and the MWR-TiO_2 NTPCs showed relatively longer electron lifetime than the TiO_2 NTPCs.

4. CONCLUSIONS

The self-doped MWR-TiO_2 NTPCs showed an efficient PEC performance because of its rational coupling of morphological and electronic features of the MWR-TiO_2 NTPCs: (1) captured light by the periodic morphological structure of the PC layer is absorbed by the self-doped interbands, (2) good electrical conductivity resulting from the high carrier density induced by Ti^{3+} doping, and (3) long photoelectron lifetime. The results of this study shed light on the rational design of photoelectrodes by coupling their morphological and electronic structures.

■ ASSOCIATED CONTENT

Supporting Information

Temperature, microwave power, and pressure profiles recorded for a sample sealed in a vessel under microwave conditions; top-view SEM image of the TiO_2 NTPCs; XPS survey of the TiO_2 NTPCs and MWR-TiO_2 NTPCs; XPS core level of Ti

dx.doi.org/10.1021/am404848n | ACS Appl. Mater. Interfaces 2014, 6, 691−696

$2p_{3/2}$ of the TiO_2 NTPCs and MWR-TiO_2 NTPCs before argon sputtering; amperometric transient photocurrent density versus time plot of TiO_2 NTs and MWRTiO_2 NTs; linear-sweep voltammograms of TiO_2 NTs and MWR-TiO_2 NTs under various conditions; photoconversion efficiency as a function of the applied potential; photocurrent densities and photoconversion efficiency of the TiO_2 NTPCs and MWR-photoelectrodes as a function of microwave reduction duration; IPCE discrepancy versus wavelength between the TiO_2 NTPCs and MWR-TiO_2 NTPCs and the correlation between UV−vis absorption and IPCE data; stability of the MWR-TiO_2 NTPCs photoelectrode; open-circuit photovoltage measurements; and electron lifetime measurements. This material is available free of charge via the Internet at http://pubs.acs.org.

AUTHOR INFORMATION

Corresponding Author

*E-mail: peng.wang@kaust.edu.sa. Tel.: +966-2-8082380.

Notes

The authors declare no competing financial interest.

ACKNOWLEDGMENTS

This work was supported by KAUST baseline fund. Z.Z. is thankful for a SABIC Postdoctoral Fellowship.

REFERENCES

(1) Zuo, F.; Bozhilov, K.; Dillon, R. J.; Wang, L.; Smith, P.; Zhao, X.; Bardeen, C.; Feng, P. *Angew. Chem., Int. Ed.* **2012**, *51*, 6223−6226.
(2) Hamdy, M. S.; Amrollahi, R.; Mul, G. *ACS Catal.* **2012**, *2*, 2641−2647.
(3) Pei, Z.; Ding, L.; Lin, H.; Weng, S.; Zheng, Z.; Hou, Y.; Liu, P. *J. Mater. Chem. A* **2013**, *1*, 10099−10102.
(4) Zheng, Z.; Huang, B.; Meng, X.; Wang, J.; Wang, S.; Lou, Z.; Wang, Z.; Qin, X.; Zhang, X.; Dai, Y. *Chem. Commun.* **2013**, *49*, 868−870.
(5) Khan, S. U. M.; Al-Shahry, M.; Ingler, W. B., Jr. *Science* **2002**, *297*, 2243−2245.
(6) Hoang, S.; Guo, S.; Hahn, N. T.; Bard, A. J.; Mullins, C. B. *Nano Lett.* **2012**, *12*, 26−32.
(7) Zhang, Z.; Yu, Y.; Wang, P. *ACS Appl. Mater. Interfaces* **2012**, *4*, 990−996.
(8) Wu, G.; Wang, J.; Thomas, D. F.; Chen, A. *Langmuir* **2008**, *24*, 3503−3509.
(9) Zhang, J.; Pan, C.; Fang, P.; Wei, J.; Xiong, R. *ACS Appl. Mater. Interfaces* **2010**, *2*, 1173−1176.
(10) Hoang, S.; Berglund, S. P.; Hahn, N. T.; Bard, A. J.; Mullins, C. B. *J. Am. Chem. Soc.* **2012**, *134*, 3659−3662.
(11) Meekins, B. H.; Kamat, P. V. *ACS Nano* **2009**, *3*, 3437−3446.
(12) Chen, X.; Liu, L.; Yu, P. Y.; Mao, S. S. *Science* **2011**, *331*, 746−750.
(13) Wang, G.; Wang, H.; Ling, Y.; Tang, Y.; Yang, X.; Fitzmorris, R. C.; Wang, C.; Zhang, J. Z.; Li, Y. *Nano Lett.* **2011**, *11*, 3026−3033.
(14) Hu, Y. H. *Angew. Chem., Int. Ed.* **2012**, *51*, 2−5.
(15) Jiang, X.; Zhang, Y.; Jiang, J.; Rong, Y.; Wang, Y.; Wu, Y.; Pan, C. *J. Phys. Chem. C* **2012**, *116*, 22619−22624.
(16) Zuo, F.; Wang, L.; Wu, T.; Zhang, Z.; Borchardt, D.; Feng, P. *J. Am. Chem. Soc.* **2010**, *132*, 11856−11857.
(17) Ohtsu, N.; Kodama, K.; Kitagawa, K.; Wagatsuma, K. *Appl. Surf. Sci.* **2010**, *256*, 4522−4526.
(18) Kimmel, G. A.; Petrik, N. G. *Phys. Rev. Lett.* **2008**, *100*, 196102−196105.
(19) Hashimoto, S.; Tanaka, A. *Surf. Interface Anal.* **2002**, *34*, 262−265.
(20) Kang, Q.; Cao, J.; Zhang, Y.; Liu, L.; Xu, H.; Ye, J. *J. Mater. Chem. A* **2013**, *1*, 5766−5774.
(21) Zhang, Z.; Hedhili, M. N.; Zhu, H.; Wang, P. *Phys. Chem. Chem. Phys.* **2013**, *15*, 15637−15644.
(22) Coffin, R. C.; Peet, J.; Rogers, J.; Bazan, G. C. *Nat. Chem.* **2009**, *1*, 657−661.
(23) Pan, L.; Liu, X.; Sun, Z.; Sun, C. Q. *J. Mater. Chem. A* **2013**, *1*, 8299−8326.
(24) Baghbanzadeh, M.; Carbone, L.; Cozzoli, P. D.; Kappe, C. O. *Angew. Chem., Int. Ed.* **2011**, *50*, 2−50.
(25) Dahal, N.; García, S.; Zhou, J.; Humphrey, S. M. *ACS Nano* **2012**, *6*, 9433−9446.
(26) Sun, Y.; Yin, Y.; Mayers, B. T.; Herricks, T.; Xia, Y. *Chem. Mater.* **2002**, *14*, 4736−4745.
(27) Kay, A.; Cesar, I.; Grätzel, M. *J. Am. Chem. Soc.* **2006**, *128*, 15714−15721.
(28) Biesinger, M. C.; Lau, L. W. M.; Gerson, A. R.; Smart, R.; St, C. *Appl. Surf. Sci.* **2010**, *257*, 887−898.
(29) Alivov, Y.; Grant, T.; Capan, C.; Iwamoto, W.; Pagliuso, P. G.; Molloi, S. *Nanotechnology* **2013**, *24*, 275704−275710.
(30) Cho, J. M.; Yun, W. J.; Lee, J. K.; Lee, H. S.; So, W. W.; Moon, S. J.; Jia, Y.; Kulkarni, H.; Wu, Y. *Appl. Phys. A: Mater. Sci. Process.* **2007**, *88*, 751−755.
(31) Czoska, A. M.; Livraghi, S.; Chiesa, M.; Giamello, E.; Agnoli, S.; Granozzi, G.; Finazzi, E.; Di Valentin, C.; Pacchioni, G. *J. Phys. Chem. C* **2008**, *112*, 8951−8956.
(32) Li, M.; Hebenstreit, W.; Diebold, U.; Tyryshkin, A. M.; Bowman, M. K.; Dunham, G. G.; Henderson, M. A. *J. Phys. Chem. B* **2000**, *104*, 4944−4950.
(33) Zhang, Z.; Zhang, L.; Hedhili, M. N.; Zhang, H.; Wang, P. *Nano Lett.* **2013**, *13*, 14−20.
(34) Zhang, Y.; Schnepp, Z.; Cao, J.; Ouyang, S.; Li, Y.; Ye, J.; Liu, S. *Sci. Rep.* **2013**, *3*, 2163-1−2163-5.
(35) Zhang, Z.; Yuan, Y.; Liang, L.; Cheng, Y.; Xu, H.; Shi, G.; Jin, L. *Thin Solid Films* **2008**, *516*, 8663−8667.
(36) Ye, M.; Gong, J.; Lai, Y.; Lin, C.; Lin, Z. *J. Am. Chem. Soc.* **2012**, *134*, 15720−15723.
(37) O'Hayre, R.; Nanu, M.; Schoonman, J.; Goossens, A. *J. Phys. Chem. C* **2007**, *111*, 4809−4814.
(38) Ghosh, P. K.; Azimi, M. E. *IEEE Trans. Dielectr. Electr. Insul.* **1994**, *1*, 975−981.
(39) Zhang, Z.; Wang, P. *Energy Environ. Sci.* **2012**, *5*, 6506−6512.